Proceedings of the
Annual Stability Conference
Structural Stability Research Council
Nashville, Tennessee, March 24-27, 2015

Post-fire buckling strength of CFS walls sheathed with magnesium oxide or ferrocement boards

Maged T. Hanna[1], JeanC. Batista Abreu[2], BenjaminW.Schafer[3], Metwally Abu-Hamd[4]

Abstract

Fire resistance is one of the most important factors to consider in the design of buildings constructed from thin-walled cold-formed steel sections. The efficiency of fire protection systems, and the stability of structural cold-formed steel studs are significantly controlled by the wall sheathing. Although gypsum wallboards are very common, other sheathing alternatives exist. This paper studiesthe fire resistance of load-bearing cold-formed steel walls sheathed with magnesium oxide and ferrocement boards. The post-fire buckling strength of cold-formed steel members is investigated experimentally and numerically. Sheathed lipped channel sections were initially exposed to fire, reaching temperatures higher than570^{o}C. Then, after cooling down, the studs were subjected to compressive loads until failure. The mechanical properties of cold-formed steel were determined after the material returned to ambient temperature, and compared with nominal values. Several member lengths were considered to account for local, distortional, and interacting local and distortional buckling modes. A parametric study based on nonlinear finite element simulations is presented. Computational models include measured geometric imperfections and temperature-dependent mechanical properties of steel. Results are compared against current design rules. This research aims to demonstrate that fire performance-based design is feasible for cold-formed steel walls with magnesium oxide or ferrocement sheathing.

1. Introduction

Recently, using of cold formed steel (CFS) sections in building constructions have shown rapid growth due to their lightness, high strength and stiffness, fast and easy erection. In building uses, the most common section is the simple lipped channel section. Inaddition, load-bearing wall panel system is the mostly used system in constructing such buildings. In this system, the vertical loads are transferred from horizontal joists to series of vertical studs; while lateral loads are resisted either by shear panels or X-bracing system.In fire condition, steel loses its strength and experienced large amount of deformations. Consequently, it is important to protect steel against fire.

[1]Associate Professor, Housing and Building National Research Center, Egypt, m_tawfick2003@yahoo.com
[2]Graduate Research Assistant, Department of Civil Engineering, Johns Hopkins University, jbatist1@jhu.edu
[3]Professor and Chair, Department of Civil Engineering, Johns Hopkins University,schafer@jhu.edu
[4]Professor, Faculty of Engineering, Cairo University,Egypt, abuhamd@eng.cu.edu.eg

Generally, fire rating is defined fora wall or floor assembly that consists of cold-formed elements sheathed with insulating boards, and itindicates the amount of timethe assembly canhelp maintaining the structural integrity of the building during fire.Several researches have studied the mechanical properties and structural behavior of cold-formed sections at elevated temperature. Ranawaka et al. (2009) developed equations to estimate the yield strength and elasticity modulus of CFS at elevated temperatures. Kankanamge et al. (2011) concluded that the steel grade has a considerable effect on the yield stress reduction at elevated temperatures. Wei and Jihong(2012) extended the work to evaluate the material properties of 1-mm-thick G550 CFS at elevated temperatures.

Feng et al. (2003)presentedtheresultsofanumerical investigationoftheaxialstrengthof cold-formed thin-walledchannelsections(columns) under non-uniform high temperatures in fire. Chen and Young (2007) showed that the column strengths predicted using finite element analysis are generally in good agreement with the test results at normal room and elevated uniform temperatures, when the reduced material properties of CFS at elevated temperatures were used. Ranawaka and Mahendran (2009) presented an experimental investigation of light gauge CFS compression members subject to distortional buckling at ambient and uniform elevated temperatures. Shahbazian et al.(2011, 2012) concluded that the DSM local and distortional buckling curves were applicable to columns with uniform temperature distributions in the cross-section. Batista and Schafer (2013) explored the elastic stability of concentrically loaded lipped channel cold-formed member subjected to non-uniform temperature distributions. They found that buckling loads decrease with increasing temperature, and rate of degradation varies according to the fire scenario. For the design of CFS studs with non-uniform temperature distributions and mechanical properties varying in the cross-section, Batista and Schafer (2014) recommendedthe use of current DSM equations with temperature-dependent mechanical properties, and the squash load computed as the product of cross-sectional area and the minimum F_y in the cross-section, similar to first yield method for beam design.

Researches have also been extended to explore the fire performance of CFSassemblies. Feng et al. (2003) found that the shape of the cross-section does not have a critical effect on temperature distributions in a steel stud panel system. Feng and Wang (2005) presented the results of eight tests on loaded full-scale cold-formed thin-walled steel structural panels. They found that, at ambient temperature, failure was due to local buckling around the top service hole while,under fire condition, the main failure mode was overall flexural–torsional buckling about the major axis. Batista et al. (2014) provides a comprehensive assessment of the current knowledge on the fire performance of CFS, and highlights the need of studying the post-fire behavior of CFS systems to enable performance-based fire design.

After fire has finished, structural engineers are always eager to know the structural efficiency of the light steel frame buildings. To answer this question the post-fire condition has to be studied.Recently, Gunalan and Mahendran (2014) found that the post-fire mechanical properties of CFS are reduced below the original ambient temperature mechanical properties if they had been exposed to temperatures exceeding 300^{o}C.Moreover, they found that CFS columns were able to regain 90% of their original distortional buckling capacities if the exposed temperature was below 500^{o}C.Inaddition, the reduction in the ultimate capacity followed a similar trend to that of yield strength.

Current design codes seem to provide reasonablepredictions of the residual compression capacities when the reduced post-fire mechanical properties are used. This paper is aiming to explore the fire rating of wall assembliessheathed with magnesium oxide and ferrocement boards. The post-fire axial strength of the lipped-channel CFSstuds has been investigated. The considered studs have several overall member slenderness ratios to study failure modes.

2. Fire Resistance Tests of Cold-Formed Sections Walls

Two fire resistance tests were carried out on load bearing walls assembly. The outer dimensions of the walls are 3020mm wide by 2720 mm height. Wallsconsisted of lipped-channel vertical studs, and were covered on both sides with 10mm thick sheets of Magnesium oxide boards (MOB) or Ferrocement boards(FCB). The cross-section of the members studied has dimensions shown in Fig. 1. The ambient temperatures at the start of the test were 28^{o}C and 38^{o}C for MOB and FCBboards, respectively. The furnace temperature was increased according to the time-temperature relationship defined in ASTM E-119. Tests were performed in theHousing and Building National Research Center (HBRC), Fire Laboratory. Recorded time-temperature curves are provided in Fig. 2.

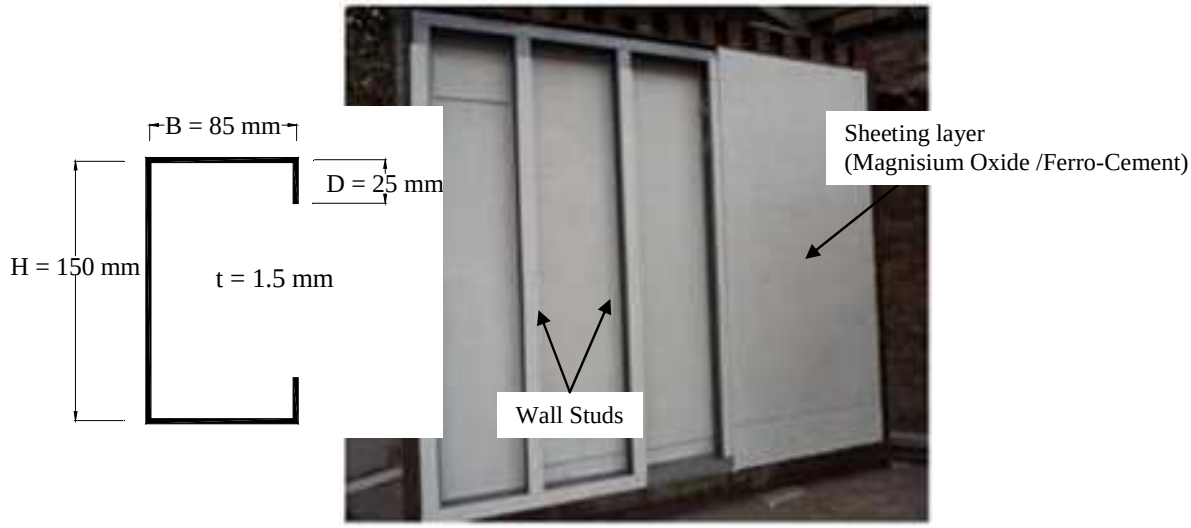

a) Stud cross section b) Wall assembly

Figure 1: Fire-resistance test samples

Several crackswere observed in the unexposed surface of the MOB wall after 40 minutes of fire exposure (Fig. 3.). However, no cracks were observed at any location on the unexposed surface of FCB, butbuckling waves were developed at different positions during the test. The wall fire rating is defined as the period after which there is a wide crack occurrence thatallows the passage of hot gases able to ignite a cotton waste placed on the unexposed side of the wall; and the amount of time until the transmission of heat through the fire test assembly is enough to raise the temperature on the unexposed surface more than 139°C above the initial temperature. These conditions happened in the MOB, and FCB after 50 minutes, and 58 minutes, respectively.

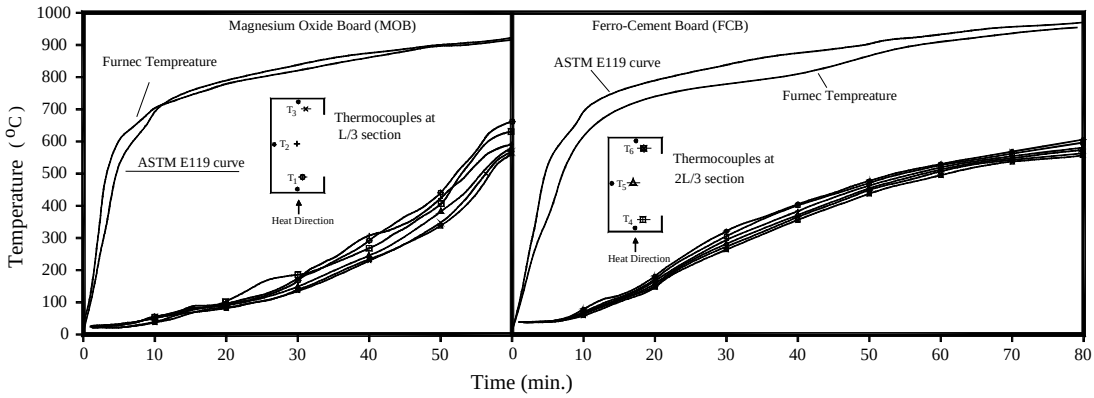

Figure 2: Time-temperature curves of the furnace and CFS studs

Figure 3: Exposed and unexposed surfaces of walls after fire test

The fire testswere allowed to continue until the average temperature of the steel reached 538^{o}C, to determine the response of CFS against fire. CFS members reached this temperature after 58 minutes, and 78 minutes in the MOB, and FCB, respectively.

3. Post Fire Strength of Walls Studs

After the fire tests were finished, the walls were left to cool down atambient temperature. Then, the vertical CFS studs were tested individually under axial compressive loads to find their residual axial capacity after being exposed to fire (i.e. post-fire case).Studs were cut into different lengths to study different failure modes.Four lengths were considered which are equal to 800, 1200, 1900, and 2700mm. Consequently, the normalized overall slenderness ratios, $\lambda_c = \sqrt{F_e/F_y}$, of the tested studs about minor axis ranged from 0.4 to 1.3.Seven tests were conducted for the post-fire case. Inaddition, two tests were done for studs that were not subjected to fire (i.e. pre-fire case). These specimens had lengths of 800mm, and 1200mm.All the tested specimens dimensions are listed in table 2.

3.1 Mechanical Properties

The mechanical properties of the CFSused in the vertical studs were determined before and after exposed to fire. The dimensions of the coupons and the test procedures were based on the ASTM-A370 specification. Specimens werecut in the longitudinal directions of the CFS sheets.Three specimens were taken from studs in the MOB wall, while two specimens werecut from FCB wall. Inaddition, two specimens were cut from studs that were not subjected to fire (i.e. pre-fire case). Fig. 4illustrates the location and nomenclatureforthe specimens. Thickness and widths of the specimens were measured by digital caliper with accuracy of 0.01 mm. Measurements were done three times at different locations for each sample. Specimens were aligned in the test machine, and tensioned at a constant rate of 1.0mm/min.

Fig. 5 shows the stress-strain curves of the tested coupons. Young's modulus "E" was determined from the slope of the initial linear part of the curve, while yield stresses was determined using 0.2% proof stress method. The results of the coupons tests are summarized in Table 1. The average yield stresses and Young's modulus of specimens at ambient temperature are 344 MPa, and 200 GPa, respectively. Results of the post-fire tests showed that there is no much loss in the Young's modulus "E" after heating; however, the yield stresses are reduced by about 25%. Gunalan and Mahendran (2014) developed a set of equations that predict the post-fire mechanical properties of low and high-grade CFS. These equations are a function of the temperature. The reduction factors of Young's modulus and the yield stresses according to these equations are also listed in table 1. It is clear that the measured values lay in the range that is defined by these equations.

a) Tensile coupons locations b) Tensile coupons after test

4: Tensile coupon specimens.

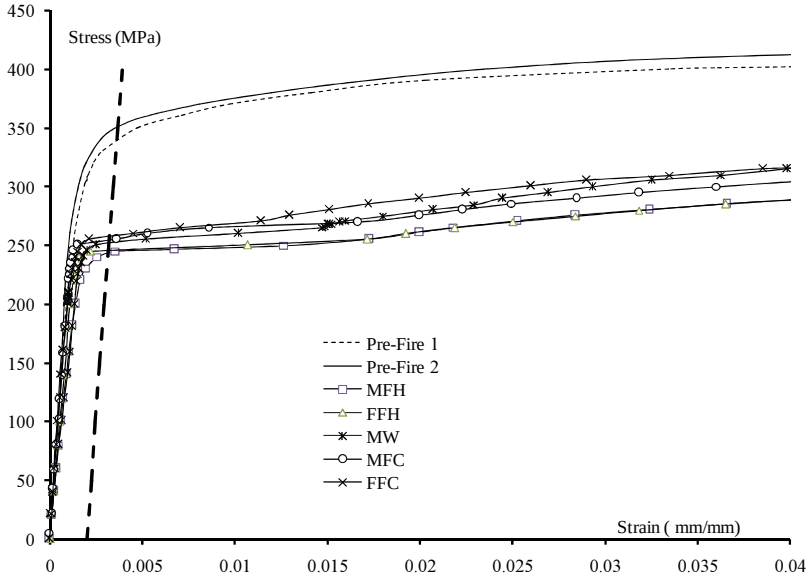

Figure 5: Stress-strain curves for the pre-fire and post-fire cases

Table 1: Tensile Coupons Test Results

Specimen	T (^{o}C)	Young's modulus, E				Yield Stresses, F_y			
		Measured values (GPa)	E_T/E	$(E_T/E)_{eqn.}$		Measured values (MPa)	F_{yt}/F_y	$(F_{yt}/F_y)_{eqn.}$	
				Low Grade	High Grade			Low Grade	High Grade
Pre-Fire 1	30	210	1.00	-------	-------	350	1.00	------	-------
Pre-Fire 2	30	205	1.00	------	-------	338	1.00	-----	-------
MFH	640	178	0.86	1	0.91	248	0.72	0.851	0.406
FFH	600	186	0.89	1	0.92	246	0.71	0.861	0.42
MW	580	190	0.91	1	0.93	255	0.74	0.865	0.45
MFC	580	200	0.96	1	0.93	258	0.75	0.865	0.45
FFC	560	210	1.01	1	0.94	262	0.76	0.87	0.5

Note: $(E_T/E)_{eqn,}$ and $(F_{yt}/F_y)_{eqn}$ values are based onGunalan and Mahendran (2014) equations

3.2 Geometric Imperfections

Geometric imperfections of the component plates forming the sections were measured by survey leveling of the specimens to an accuracy of 0.01mm per reading. All component plates of the specimens were divided into grids consisting of three equally spaced lines on each flange and three on the web. These led to 10 lines to measure the imperfections across the section, as depicted in Fig.6. Seven equally spaced cross-sections were taken along the specimen. The specimens were placed on a nearly horizontal table. Inclination of the table between the start and the end of the specimens was determined and eliminated from the readings.Local imperfections, δ_L, demonstrate the out of flatness in the plate elements forming the section, and it is calculated by subtracting the readings taken at the middle points from the average of the readings at the two end points of each plate elements. However, distortional imperfections, δ_d, reflect the translation of one plate end with respect to the other end.

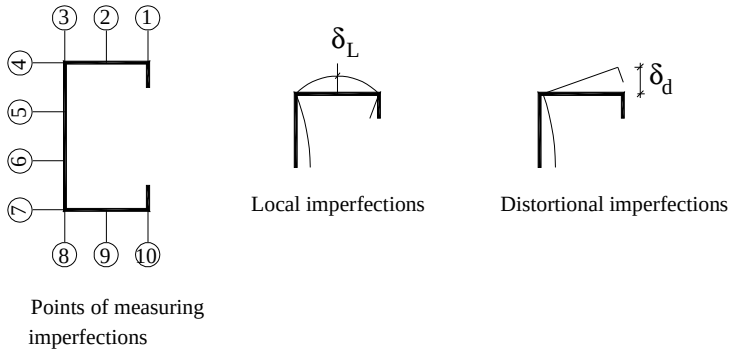

Figure 6: Geometric imperfections

Due to exposure to high temperature, the specimens experienced thermal deformations.This led to large values of geometric imperfections.Results indicated that the average local imperfections, δ, are0.8t and 1.8t for the flanges and web, respectively. However, the average distortional imperfections are 2.8t in the flanges, and 1.6t in the web. In addition, the average overall geometric imperfections, Δ, about major and minor axis are L/1400 and L/890, respectively.

3.3 Test Setup

Specimens weretested vertically in a 500t capacity testing machine as shown in Fig. 7. Two thick plates with thickness of 15 mm were connected at the ends of each specimen. Cold-formed sections with dimensions smaller than that of the original stud were welded to the head plate, and then bolted to the CFS stud. The thickness of these sectionswas 5mm(see Fig.7). The load wasapplied to the specimens through hinges placed in a groove made to thick end plates. These end conditions allow rotation about strong and weak axis, while preventing horizontal displacement of the specimen. Moreover, the presence of head plates prevents warping deformations of the specimen end-sections.

Specimens were aligned in the machine so that the loads were applied through the centroid of the section. The shift of the point of applied load from the section centroid was measured before test. Lateral displacements of the specimens were measured through linear variable displacement transducers (LVDT) with accuracy of 0.01 mm. The measured points were the flange-lip juncture points as well as the web central point. These points were located at the mid-height section of the studs. The LVDT readings were collected using a data acquisition system. An arbitrary increment of load equal to 5kN was applied, and then the load was held constant until stable readings were recorded. This procedure was repeated for each additional load increment until excessive deflection was observed without any increase in the applied load. Thus, the ultimate load was achieved.

The applied load, P, was normalized with respect to the squash load of the cross section at the original ambient temperature (i.e. $P_y = A*F_y$, with F_y = 340 MPa). The normalized ratios (P/P_y) have been plotted against the lateral displacements of the three points at the mid-height section of specimens L120, and FL120-2 in Fig. 8. In addition, the horizontal displacements of the web central point were plotted as a function of the normalized ratios of P/P_y in Fig. 9 for all the tested samples. The measured dimensions of the tested specimens and test results are listed in Table 2.

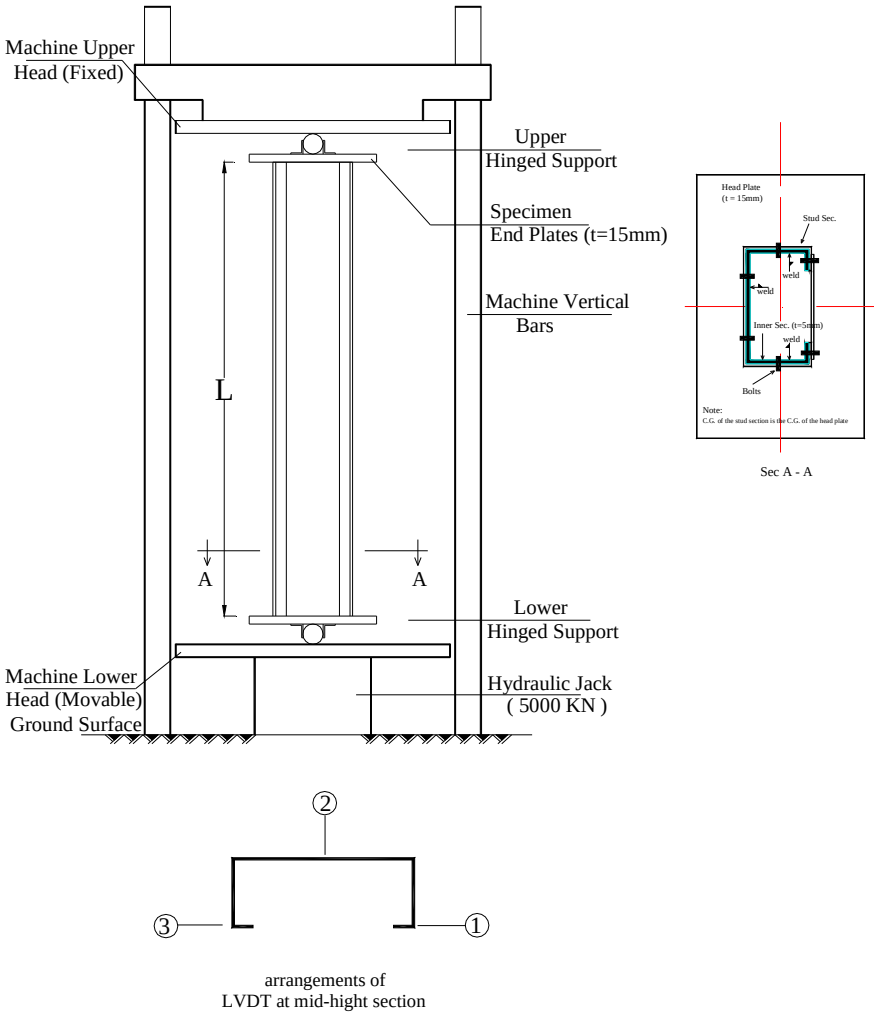

a) Test Machine b) Test setup

Figure 7: Test Setup

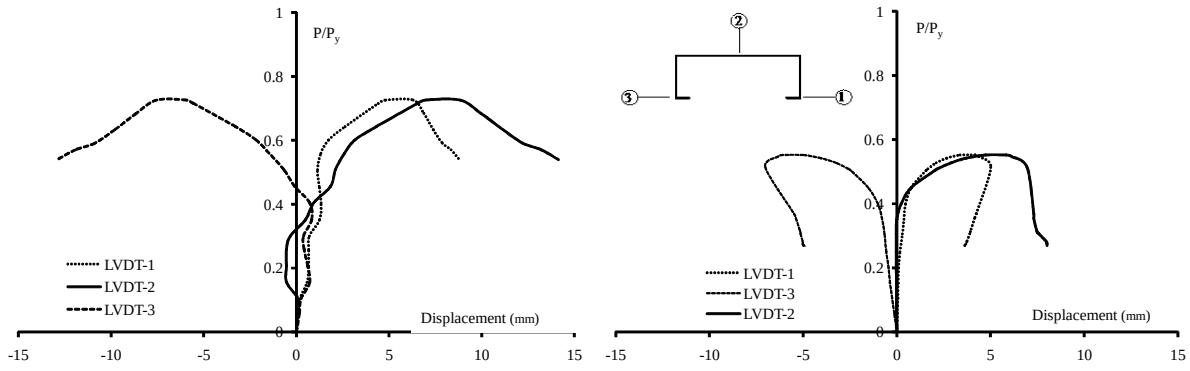

a) Pre-fire case b) Post-fire case

Figure 8: Load horizontal displacements of specimens with length L = 1200mm

For the pre-fire samples, the failure mode observed was distortional buckling of the flanges. However, for short specimen (i.e. L=800mm) there were slight local buckling waves in the web in conjunction with the distortional movement of the flanges. In the early stages of loading, there were slight displacementsof the flanges and web. Then, as soon as the sectional buckling occurred, there was a significant increase of the horizontal displacements of the flanges and web (Fig. 9). Moreover, the flanges rotated toward the web quite symmetrically about the vertical axis of the specimens. Similarly, the failure modes of the post-fire short length specimens (i.e. L = 800, 1200 mm) were characterized by distortional buckling of the flanges. However, there were unsymmetrical movements of the flanges about the vertical axisdue to the change of the mechanical properties across the cross section. This is clearly shown in Fig. 8. The failure modes of specimens L120, and FL120-2 are depicted in Fig. 11, and Fig. 12, respectively. Moreover, the post-fire ultimate loads of short specimens are 25% lower than the ambient ultimate loads.

The long specimens showed overall bending deformations about the section minor axis; therefore, the load-displacement relationships increased continually up to failure. The failure mode of specimen ML270 was overall flexural-torsional buckling associated with local buckling waves in the web and flanges, see Fig. 13.

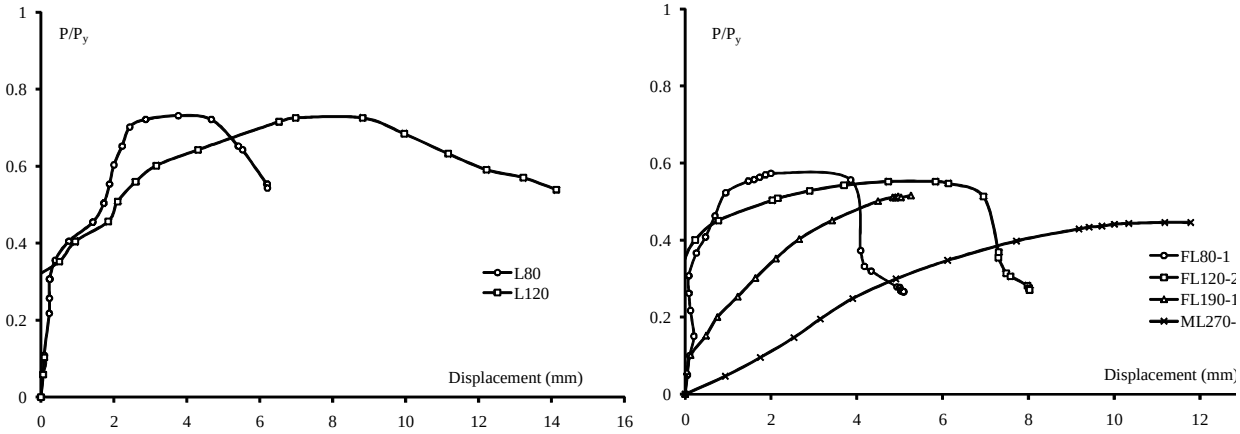

a) Pre-Fire b) Post-Fire

Figure 9: Load-horizontal displacement of the tested specimens web central point.

Table 2: Test specimen dimensions and results

Specimen Name	Board Name	L (mm)	Measured Dimensions (mm)				Experimental		FEM			
			H	B	D	t	P_u (KN)	$\frac{P_u}{P_y}$	P_{cr} (KN)	$\frac{P_{cr}}{P_y}$	P_u (KN)	$\frac{P_u}{P_y}$
L80	------	800	149.5	84.7	26.6	1.65	152	0.73	89	0.43	155	0.74
L120	------	1200	150.3	85.6	27.5	1.72	150	0.72	93	0.45	151	0.73
FL80	FCB	800	149.3	85.1	27.4	1.65	119	0.57	77	0.37	120	0.57
ML120	MOB	1200	148.8	84.8	28.1	1.73	110	0.52	86	0.41	122	0.58
FL120-1	FCB	1200	150.9	83.3	26.6	1.66	103	0.49	86	0.41	122	0.58
FL120-2	FCB	1200	150.6	83.4	26.6	1.75	113	0.54	86	0.41	122	0.58
ML190	MOB	1900	149.4	84.7	27.5	1.73	103	0.49	81	0.39	116	0.55
FL190	FCB	1900	150.6	84.6	27.1	1.73	103	0.49	81	0.39	116	0.55
ML270	MOB	2700	150.1	84.9	27.5	1.75	93	0.44	44	0.21	103	0.49

Note, $P_y$is the pre fire squash loads of the cross section

3.4 Numerical Finite Element Model

A nonlinear finite element model was developed in COSMOS/M to simulate the tested specimens. The full length of the specimens was modeled so that the axis of the specimen coincides with the vertical Y-axis while the lateral displacements lie in the X-Z plane as shown in Fig. 10. Four-nodeisoparametric shell elements(shell 4T) that allow for both geometric and material nonlinearitieswere used. The mesh density was chosen such that the element aspect ratio on average equaled one. The four corner points at the two end sections were prevented from horizontal translation along X and Z directions. Loads were applied at one end through the centroid of the specimens. The loading point was also prevented from horizontal translation along X and Z directions; however, the corresponding point on the other end was prevented from translation along X,Y, and Z directions. End plates with thickness 20 mm were added at both ends of the model.

For the pre-fire case, the yield stresses and Yong's modulus "E" are taken equal to 340 MPa, and 200 GPa; respectively. However, for the post-fire cases, the mechanical properties were varied across the cross-section with the pattern shown in Fig. 10. This was based on the values calculated in sec 2.2. It was assumed that the flange and the lip as well as portion of the web with width equal to the lip width have the same properties. However, the middle part of the web will have slightly different properties. The material behaviorwas assumed to be elastic-perfectly plastic obeying von Mises yield criterion. Overall geometric imperfections were included in the model by assuming the member bent about the minor axis in a half sine wave. Two imperfection values equal to L/1000 and L/500 are assumed. Moreover, flange distortional imperfectionswere also considered in addition to the overall imperfections. Valuesof distortional imperfections were taken equal to 3t. The load was increased according to a pre-defined time curve using the load control technique.

The experimental load versus lateral displacements of the web central point at mid height section curves are plotted together with those obtained from the finite element model. These relations are shown in Fig. 11, Fig. 12, and Fig. 13 for specimens L120, FL120-2, and ML270, respectively. The overall imperfections value "L/500" was applied in two directions. The first direction causes compression on the lip, while the second direction causes compression on the web.

Figures show that the increase of the overall geometric imperfections leads to excessive overall deformations and slight decrease in the ultimate loads. When the overall imperfection increases from L/1000 to L/500 the ratio P_u/P_y for specimen L120 decreases from 0.74 to 0.67. Similarly, this ratio for specimen FL120-2 changes from 0.59 to 0.56. Moreover, for specimens L120, and FL120-2, when the overall imperfection is applied in the direction that causes compression in the lip, the failure mode is distortional buckling, and the flanges move toward the web. On the other hand, the failure mode changes to local buckling of the web, and the flanges move out of the web when the mode of imperfection causes compression in the web. In addition, the ultimate loads in the second case are slightly higher than the case when lips are in compression. The numerical and experimental failure modes of specimens L120, and FL120-2 are depicted in Fig. 11 and Fig.12, respectively. Failure mode of long specimen ML270 is overall flexural-torsional buckling, see Fig.13. Numerical ultimate loads and elastic buckling loads of the specimens are listed in Table 2. In general, there is good agreement between numerical and experimental results.

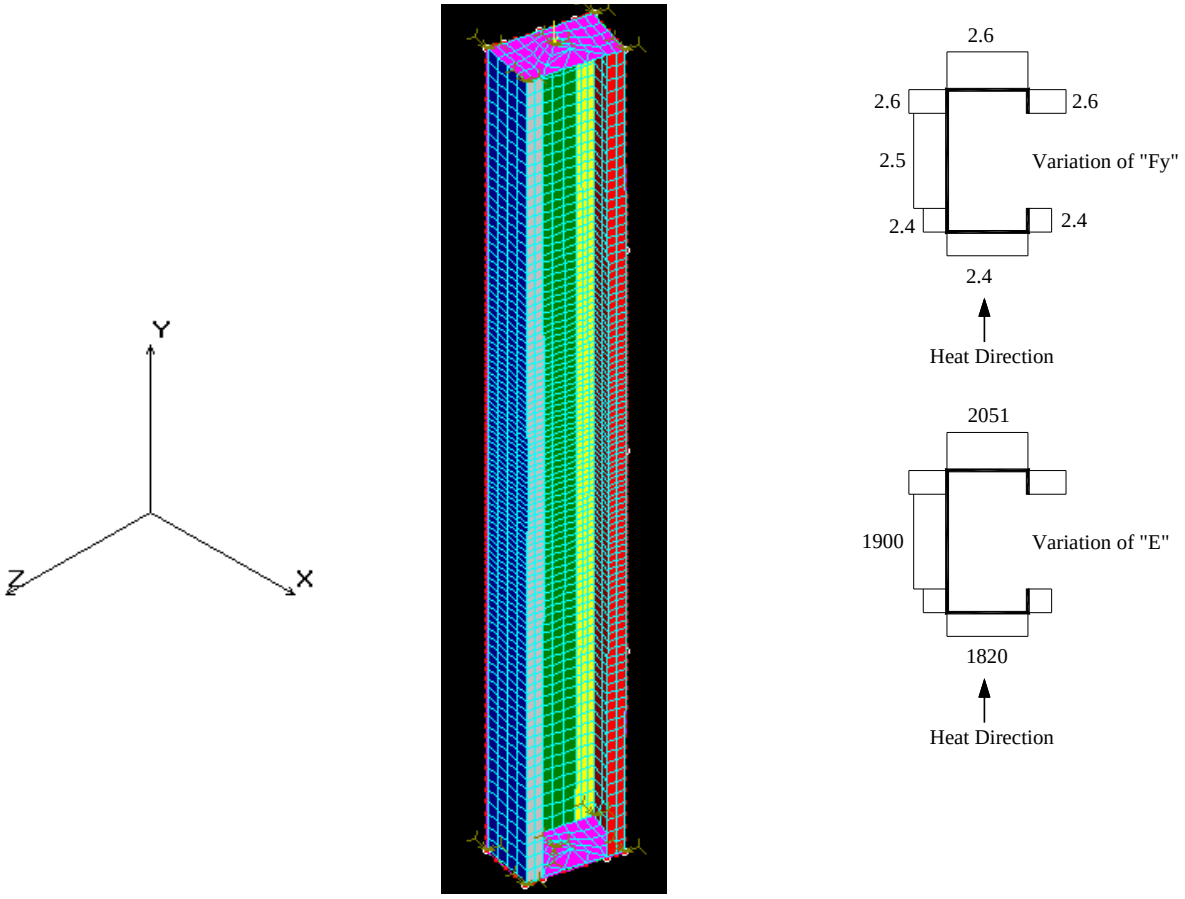

Figure 10: Finite element model

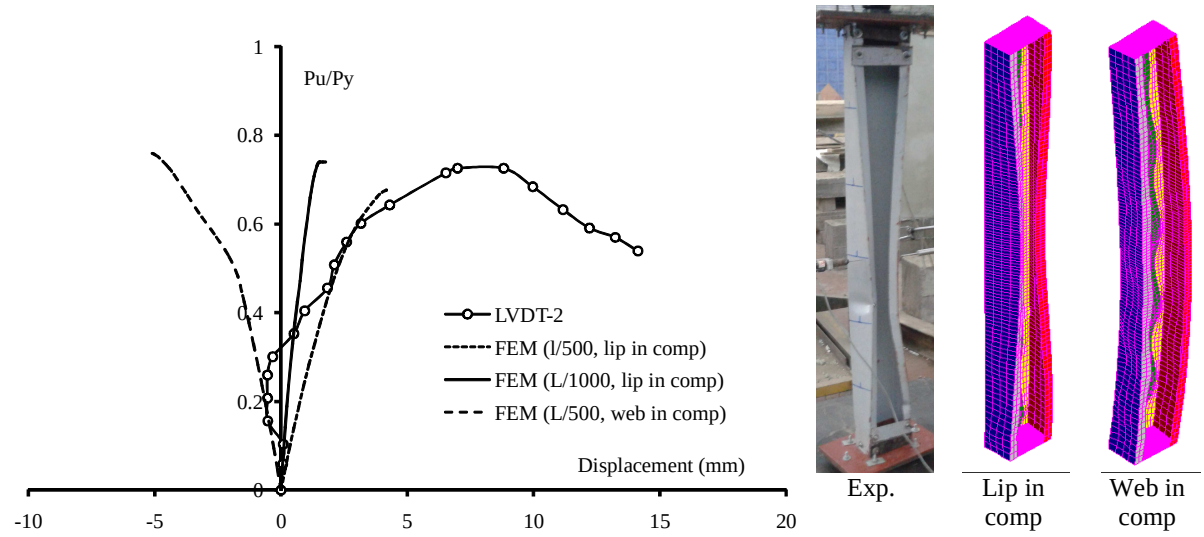

Figure 11: Load-horizontal displacements of web central point and modes of failure of specimen L120 (pre-fire)

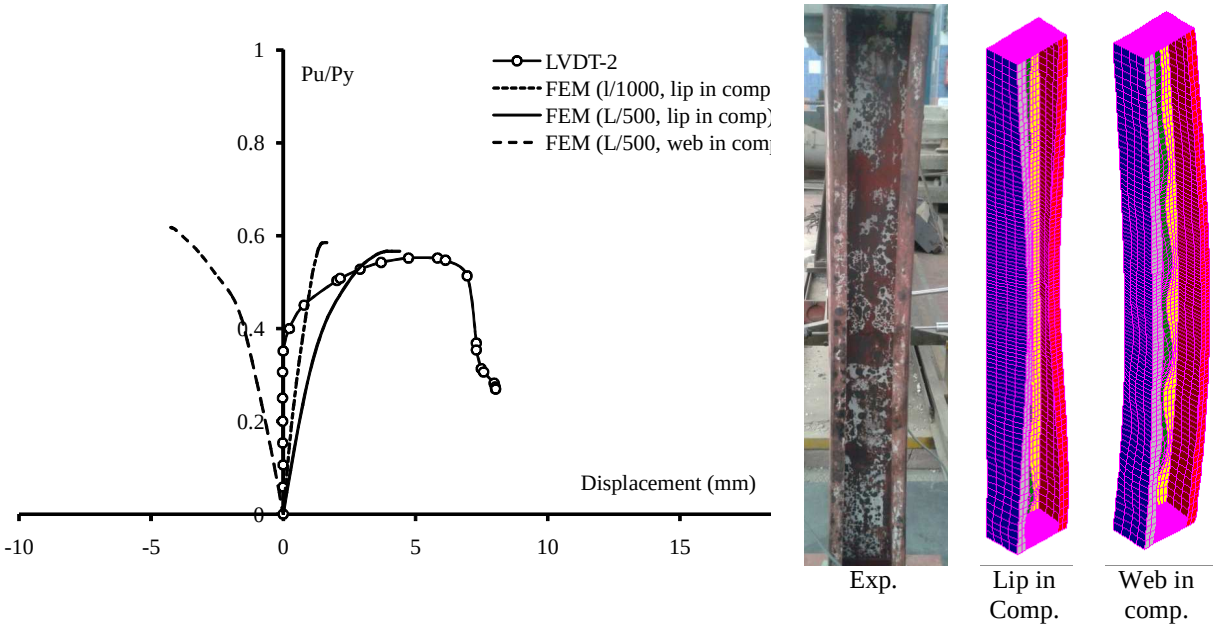

Figure 12: Load-horizontal displacements of web central point and modes of failure of specimen FL120-2

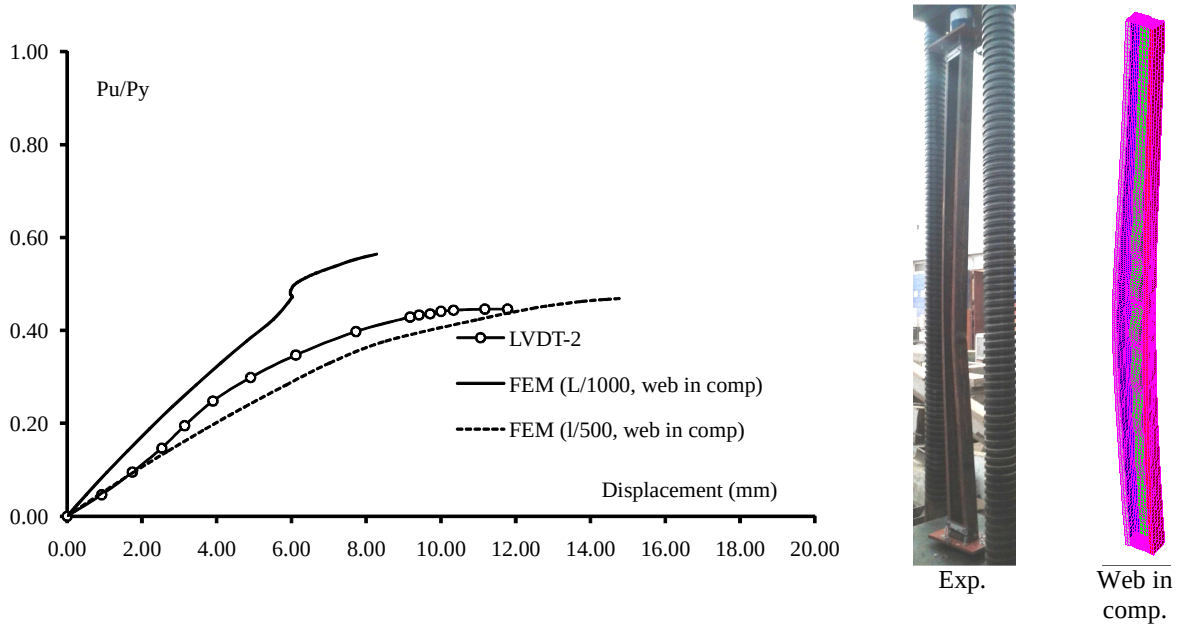

Figure 13: Load-horizontal displacements of web central point and modes of failure of specimen ML270

4. Comparison with Design Codes

The experimental ultimate loads of the studs, P_u, were compared against predictions from design rules of the Direct Strength Method "*DSM*" by Schafer (2002),as well as the*AISI-2012*equations. DSM requires the calculation of the elastic critical local and distortional buckling stresses. These values were determined using CUFSM computer program. In *AISI-2012*, the capacity of the columns is calculated as the product of the cross section effective area, A_e, and the maximum stress, F_n. The later will be the minimum of the yield stresses or flexural buckling stresses, which is determined using the full section properties.

The signature elastic buckling curve of the studied cross section is shown in Fig. 14 for the pre-fire and post-fire cases. The vertical axis represents the normalized ratios of P_{cr}/P_y, where P_y is the squash loads of the pre-fire case. Notice the used material properties werebased on experimental results. Further, for the post-fire case, the variation of the mechanical properties across the cross-section shown in Fig.10wasdefined in the finite strip model. Resultsreveal that there is slight drop in the critical local and distortional buckling loads since the local and distortional loads are decreased by 8%, and 9%, respectively. This can also be conclude from results in table 2, since the variation in elastic buckling loads between the pre-fire and post fire cases is only 10%. Moreover, there is no difference in the buckling mode shapes.

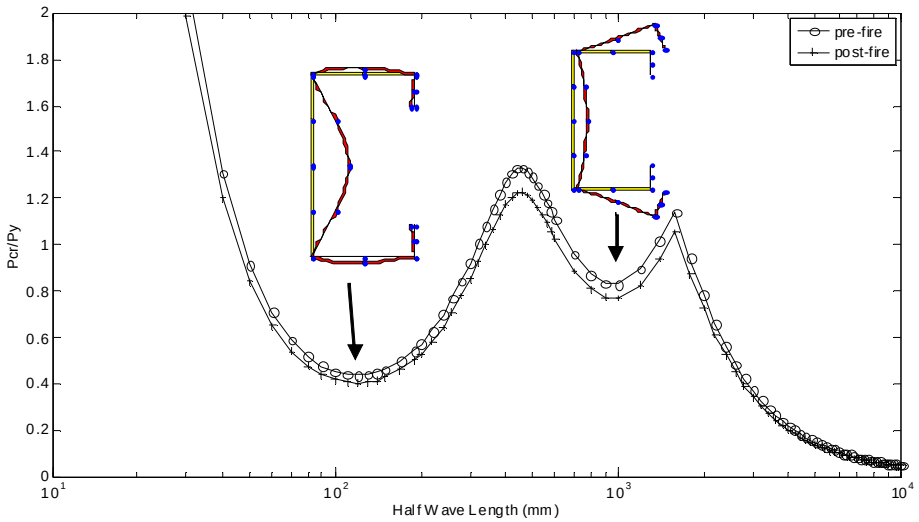

Figure 14: Elastic buckling loads of the CFS studs

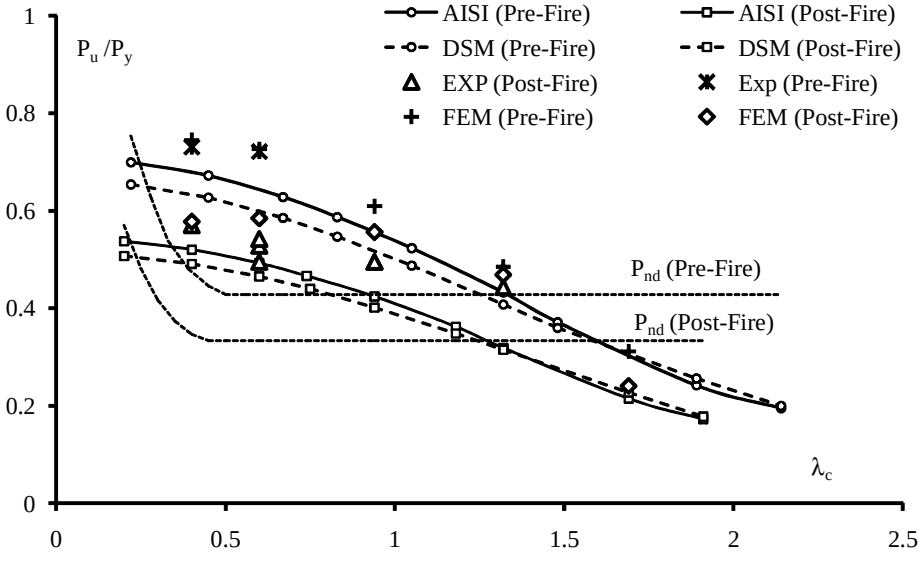

Figure 15: Comparison of the results with the predicted values of DSM and AISI-2012

The design loads calculated according to DSM and *AISI-2012* are plotted as function of the normalized slenderness ratio, $\lambda_c = \sqrt{F_e/F_y}$ in Fig.15. Note that, F_e is overall elastic buckling stresses, and F_y is yield stresses that corresponds to the pre-fire or post fire cases. Inaddition, the distortional buckling strength, P_{nd}, has been included in *AISI-2012* as limiting strength of lipped channel cross-section columns (provision C4.2). The partial safety factors, γ_{M1} and ϕ_c, werenot included when calculating the design loads. The finite element model wasused to determine the ultimate loads of columns with larger overall slenderness ratios. These results are also added to the figure. It is clear that both DSM and AISI-2012 conservatively predict the ultimate loads. However, the AISI-2012 gives results a slightly higher than DSM. It is interesting that short and intermediate slender columns lose 25% of theiroriginal capacity when they cool down after fire. However, slender columns ($\lambda_c > 1.5$) where failure is mainly overall buckling the reduction in strength become 15%. This illustratesthatthe failure of long columns mainly depends on Young's modulus "E", which is not greatly changed after fire compared with the yield stresses.

5. Conclusions

The post-fire axial strengths of lipped channel cold-formed sections have been studied experimentally. First, tensile coupons results revealthat there is no much loss in the Young's modulus "E" from the original ambient temperature values. However, the yield stresses are reduced by about 25%. Before tests are carried out the specimens geometric imperfections were measured. Due to the thermal expansions during fire, the specimens developedhigh levels of imperfections.The post-fire specimens failure modeswerecharacterized by distortional buckling of the flanges for short columns, and overall flexural torsional buckling associated with local buckling waves in the web and flanges for long columns.Moreover, the specimens have been modeled numerically using nonlinear finite element model.Numerical results reveal that when the overall imperfection is applied in the direction that causes compression in the lip, the failure modes are distortional bucklingof the flanges. On the other hand, the failure mode changes to local buckling of the web when the imperfection mode causes compression in the web. In addition, the ultimate loads in the second case are slightly higher than the case when lips are in compression.Both, the experimental and numerical results, indicate that short and intermediate slendercolumns lose about 25% of theiroriginal load-carrying capacity when they cool down after fire. However, for slender columns ($\lambda_c > 1.5$), the reduction in strength becomesonly 15%. Finally, results are compared with the predicted strength of *AISI-2012*, and the *DSM*. Comparison showed that the design specifications conservatively predict the ultimate loads.

Acknowledgments

The authors gratefully acknowledge the support of the EgyptianScience and Technology Developing Fund(STDF) for supporting this work under grant No. 5849.

References

AISI (2012), Cold-formed steel design manual, American Iron and Steel Institute, AISI

ASTM A370, "Standard Test Methods and definitions for mechanical testing of steel products".

ASTM E119, "Standard Test Methods for Fire Tests of Building Construction and Materials"

Batista Abreu J.C., Schafer, B.W. (2013). "Stability od cold-formed steel compression members under thermal gradients", *Proceedings of the Annual stability Conference,Structural stability research council*, St. Louis Missouri, April 16-20.

Batista Abreu J.C., Schafer, B.W. (2014). "Stability and load-carrying capacity of cold-formed steel compressionmembers at elevated temperatures",*Proceedings of the Annual stability Conference,Structural stability research council*, Toronto, ON, March25-28.

Batista Abreu J.C., Vieira L.C.M., Abu-Hamd M., Schafer B.W. (2014),"Review: development of performance-based fire design for cold-formed steel", Fire Science Reviews 3 (1):1

Chen, J., Young, B. (2007),"Cold-formed steel lipped channel columns at elevated temperatures. *Engineering Structures*,29, 2445–2456.

COSMOS/M V2.6, (2000), "Structural Research and Analysis Corporation", S.R.A.C, Los Angeles, CA

CUFSM V3.12, "Elastic Buckling Analysis of Thin-Walled Members by Finite Strip Analysis", http://www.ce.jhu.edu/bschafer/cufsm

Feng M., Wang Y.C., and Davies J.M. (2003)"Axial strength of cold-formed thin-walled steel channels under non-uniform temperatures in fire".*Fire Safety Journal*,38(8): p. 679-707.

Feng M., Wang Y.C. and Davies, J.M. (2003)"Thermal performance of cold-formed thin-walled steel panel systems in fire",*Fire Safety Journal*, 38, pp. 365–394

Feng, M. and Wang Y.C. (2005),"An experimental study of loaded full-scale cold-formed thin-walled steel structural panels tested under fire conditions*", Fire Safety Journal*, 40, pp. 43-63.

Gunalan, S., Mahendran, M. (2014). "Experimental investigation of post-fire mechanical properties of cold formed steel." *Thin-Walled Structures*, (84) 241-254

Gunalan, S., Mahendran, M. (2014). "Experimental and numerical studies of fire exposed lipped channel columns subject to distortional buckling" *Fire Safety Journal*, (70) 34-45.

Kankanamge N.D., Mahendran M. (2011), "Mechanical properties of cold-formed steels at elevated temperatures"*Thin-Walled Structures*, 49(1): p. 26-44.

Ranawaka T., Mahendran M. (2009), "Experimental study of the mechanical properties of light gauge cold-formed steels at elevated temperatures.*Fire Safety Journal*,44(2): p. 219-229.

Ranawaka, T., Mahendran, M. (2009), "Distortional buckling tests of cold-formed steel compression members at elevated temperatures". *Journal of Constructional Steel Research*,65, 249–259.

Schafer BW, "Design Manual for the Direct Strength Method of Cold-formed Steel Design", Final Report to the American Iron and Steel Institute, Washington, DC, 2002

Shahbazian A., Wang Y.C. (2011), "Application of the Direct Strength Method to local buckling resistance of thin-walled steel members with non-uniform elevated temperatures under axial compression"*Thin-Walled Structures*,49(12): p. 1573-1583.

Shahbazian A.,Wang Y.C. (2012), "Direct Strength Method for calculating distortional buckling capacity of cold-formed thin-walled steel columns with uniform and non-uniform elevated temperatures".*Thin-Walled Structures*,53: pp. 188-199.

Wei C., Jihong Y. (2012),"Mechanical properties of G550 cold-formed steel under transient and steady state conditions",*Journal of Constructional Steel Research*, (73) 1–11.